# 3D Numerical Simulations of Spherical Flames Instability and Acceleration in Shock Accelerated Flows

Yuejin Zhu, Gang Dong*, Baochun Fan, Yixin Liu
State Key Laboratory of Transient Physics, Nanjing University of Science and Technology
Nanjing, Jiangsu, China

## 1 Introduction

A flame in the unburned fuel/oxide mixture subjected to shock acceleration is usually unstable. This phenomenon mainly involves the Richtmyer-Meshkov (RM) instability which is produced by baroclinic effect due to the misalignment between pressure gradient and density gradient. The RM instability can result in the vorticity deposition in flame surface and greatly promote the mixing of fuel/oxide and the acceleration of the flame. Therefore, flame instability in the shock accelerated flow is practically significant in the supersonic combustion propulsion applications and safety problems. A typical scenario of flame instability in the shock accelerated flows is the interaction between the flame and shock waves. This interaction has been widely investigated experimentally (e.g., [1-2]) and numerically (e.g., [3-9]). These studies show that an initial spherical or cylinder flame undergoes the shock compression and subsequent distortion when an incident shock wave passes through the flame. During the interaction, the RM instability process is the dominant mechanism [4-5, 9] for flame instability. If the stronger wave reflected from end wall of shock tube interacts with the distorted flame again, the flame can be greatly disturbed and accelerated [2, 8]. In this case, a complex reactive shock bifurcation (RSB) structure (also called "strange wave" structure [7]) may emerge via the wave-flame-boundary layer interactions [2, 6-7]. Further, the RSB structure can result in the formation of one or more hot spots that lead to a detonation. However, most of numerical studies focus on the 2D or 2D axisymmetric shock-flame interaction, only a few reports exist on 3D shock-flame interaction [6]. Although experimental measurements are performed in 3D shock tube, but they only provide the photographs of a 2D optical projection for shock-flame complex [1, 2]. Because the instability and acceleration of flame are intrinsically 3D, the spatio-temporal characteristics of flame evolution (e.g. hot spots formation) strongly depend on the real 3D structure such as RSB or strange wave [2, 6].

In the current study, the 3D numerical simulations are performed to investigate the spherical flame evolution in shock accelerated flow. The main aim is to study the effects of incident shock wave strength and spherical flame number on the flame instability and acceleration.

## 2 Numerical Model

The three-dimensional reactive Navier-Stokes equations coupled with one-step Arrhenius chemical reaction are employed to simulate the shock-flame interaction on the uniform hexahedral meshes. The PPM scheme with TVD property and third-order spatial accuracy [10] is used to approximate the numerical flux of the advection term. The central difference scheme is applied to solve the viscous

Correspondence to: dgvehicle@yahoo.com

terms. A second-order Runge-Kutta time marching is adopted for unsteady problems in present simulations. The computational setup is an analogue of the test section of a shock tube experiment described by Thomas et al. [2]. The three-dimensional computational domain represents a quarter of tube cross-section with 170mm in length ($x$), 38mm in height ($y$) and 19mm in width ($z$). The uniform cell size is $\Delta x=\Delta y=\Delta z=0.38$mm, which represents 2 times smaller than the reaction zone of laminar ethylene/oxygen/nitrogen flame propagation under the condition studied. Although it can not fully resolve the detonation wave structure, but it is enough for correctly describing flame development, shock bifurcation and flow field in the vicinity of hot spot formation. The one-step Arrhenius reaction describes the ethylene chemistry in the $C_2H_4+3O_2+4N_2$ medium at $T_0$= 293K and $P_0$=13.3kpa, which are identical to those in Thomas' experiment [2]. The one-step reaction rate is

$$\dot{\omega} = A\rho Y \exp\left(-\frac{E_a}{RT}\right)$$

where $A$ is the pre-exponential factor, $\rho$ is the density, $Y$ is the mass fraction of ethylene, $E_a$ is the activation energy, $R$ is the universal gas constant, and $T$ is the temperature. The value of $E_a$ is set to $38.2RT_0$ according to the [11], the value of $A=1.2\times10^8$ is selected to ensure half-width size of reaction zone, $x_d$=0.3mm, which matches the experimental detonation cell size ($\lambda$=15mm) for $C_2H_4+3O_2+5N_2$ medium at the $P_0$=20kpa [12], that is, $\lambda \approx 50x_d$. In addition, the chemical heat release, $Q=39.76RT_0/M$, and adiabatic index of system, $\gamma$=1.256, are determined in terms of the method in [13]. In the simulations, an ideal gas assumption is adopted, the transport coefficients (viscosity, conductivity and diffusivity) are exponentially dependent on the temperature and Lewis number equals to unity.

# 3 Results and Discussions

In present study, three different initial conditions for shock-flame interaction are considered, see Table 1. Note that two initial spherical flames in case 2 align in shock movement ($x$) direction, the initial total volume ($V_0$) of the flames is same as those in case 1 and 3 but the initial total surface area of the flames is larger than those in case 1 and 3.

In the first computation (case 1), a spherical flame bubble with initial radius of 19 mm is used to interact with a planar incident shock wave with Ma=1.7 and its reflected wave. For validating the numerical scheme and chemical reaction model， the computational Schlieren images from three-dimensional numerical results are produced by using following equations[6]:

$$I_{x-y} = I_0\left[\left(\int \frac{\partial \rho}{\partial x} dz\right)^2 + \left(\int \frac{\partial \rho}{\partial y} dz\right)^2\right]^{\frac{1}{2}}$$

where $I_{x-y}$ and $I_0$ are the computational $x$-$y$ plane and initial light intensities, respectively. Figure 1 shows the comparisons of the spherical flame instability between the experimental [2] and computational images at the selected times. Figs. 1(a)-(c) correspond to the interaction between the incident shock wave and flame, while Figs. 1(d)-(f) correspond to the interaction between the reflected shock wave and distorted flame. Computational Schlieren image represents the three-dimensional projection of light on the $x$-$y$ plane and thus reflects the real complex structure of distorted flame. The good qualitative agreements between the measured and calculated results are obtained.

Table 1: Initial conditions of shock-flame interactions

| Type | Incident Shock Mach number | Spherical flame number | Single flame radius, m | Single flame surface area, $m^2$ | Single flame volume, $m^3$ |
|---|---|---|---|---|---|
| Case 1 | 1.7 | 1 | 0.019 | $4.536\times10^{-3}$ | $2.873\times10^{-5}$ |
| Case 2 | 1.7 | 2 | 0.0151 | $2.865\times10^{-3}$ | $1.4365\times10^{-5}$ |
| Case 3 | 2.1 | 1 | 0.019 | $4.536\times10^{-3}$ | $2.873\times10^{-5}$ |

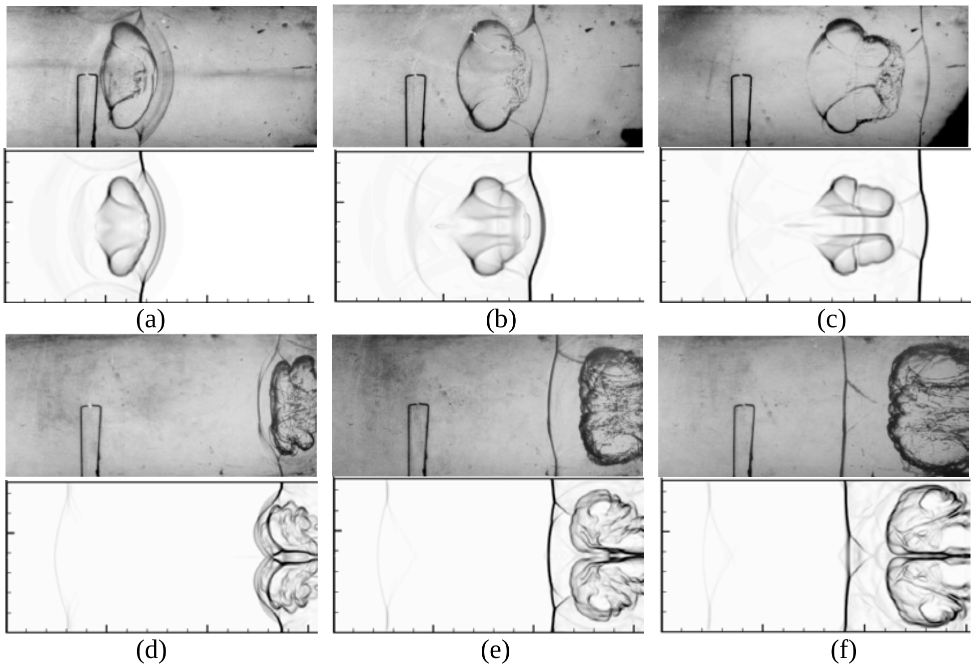


Figure 1. Comparisons of experimental and computational Schlieren images. The details of experiments are described by [2]. The incident shock wave with Ma=1.7 travels from left to right.

Figure 2 gives instantaneous slices of ethylene mass fraction distributions and pressure contours in the *x*-*y* plane and *x*-*z* plane for three cases (see Table 1) after reflected wave has interacted with distorted flames. For case 1 in Fig.2 (a), the spherical flame has been greatly distorted at $t$=515μs after the reflected wave has passed through the single flame. While for case 2 in Fig.2 (b), two distorted flames has been united each other induced by reflected wave at $t$=515μs. In this case, a partial coupling between the reflected wave and the flame front is observed on window slice in *x*-*y* plane. From *x*-*z* plane view, the coupling is the reactive shock bifurcation (RSB) structure, which is attached on the window plane in the vicinity of the symmetry plane. This attachment is due to the mutual induction of two flames and the larger total flame surface area which make flames enter the recirculation zone of RSB. The propagating velocity and pressure of the RSB structure are about 740m/s in laboratory coordinates and 160kpa, respectively, which are far smaller than those of detonation wave structure ($D_{CJ}$=2027m/s and $P_{CJ}$=680kpa in the incident shock gas with Ma=1.7). For stronger incident shock wave case, significantly different results from Figs. 2(a) and 2(b) can be found in Fig. 2(c). In this case, the flame rapidly expands and a nearly full coupling between the reflected wave and flame front is visible in the window slice in *x*-*y* plane at shorter time, $t$=415μs. In the *x*-*z* slice, the RSB structure corresponded to the strong coupling is observed on the slice of $y$=0.019m. The propagating velocity and pressure of the RSB structure are about 1113m/s and 400kpa, which are 55% of CJ detonation velocity and 44% of the CJ detonation pressure ($D_{CJ}$=2031m/s and $P_{CJ}$=901kpa in the incident shock gas with Ma=2.1). Thus, it is confirmed that the RSB is that of "strange wave" [2]. In addition, detonation events D1 and D2 are observed. The occurrences of the detonations are related to the formation of hot spots. For example, Fig. 3 shows a formation of a hot spot that induces D2 at the somewhat early time, $t$=406μs, for case 3. A pocket of unburned mixture behind the reflected wave is enveloped by flame zones 1-3 and window plane. Zone 1 is the flame within the recirculation zone of RSB as shown in Fig. 2(c), zone 2 is the distorted flame induced by reflected wave, and zone 3 is the flame within another small RSB structure. The convergence and collision of the compressed waves of flame fronts within these zones produce a hot spot with high density and pressure, which finally leads to a detonation as shown in Fig. 2(c). The mechanism and location of formation of hot spot in case 3 are different from 3D simulation by [6]. Similarly, a hot spot that induced D1 forms in a pocket of unburned mixture near the corner between wall of $y$=0m and end wall of shock tube (not shown here).

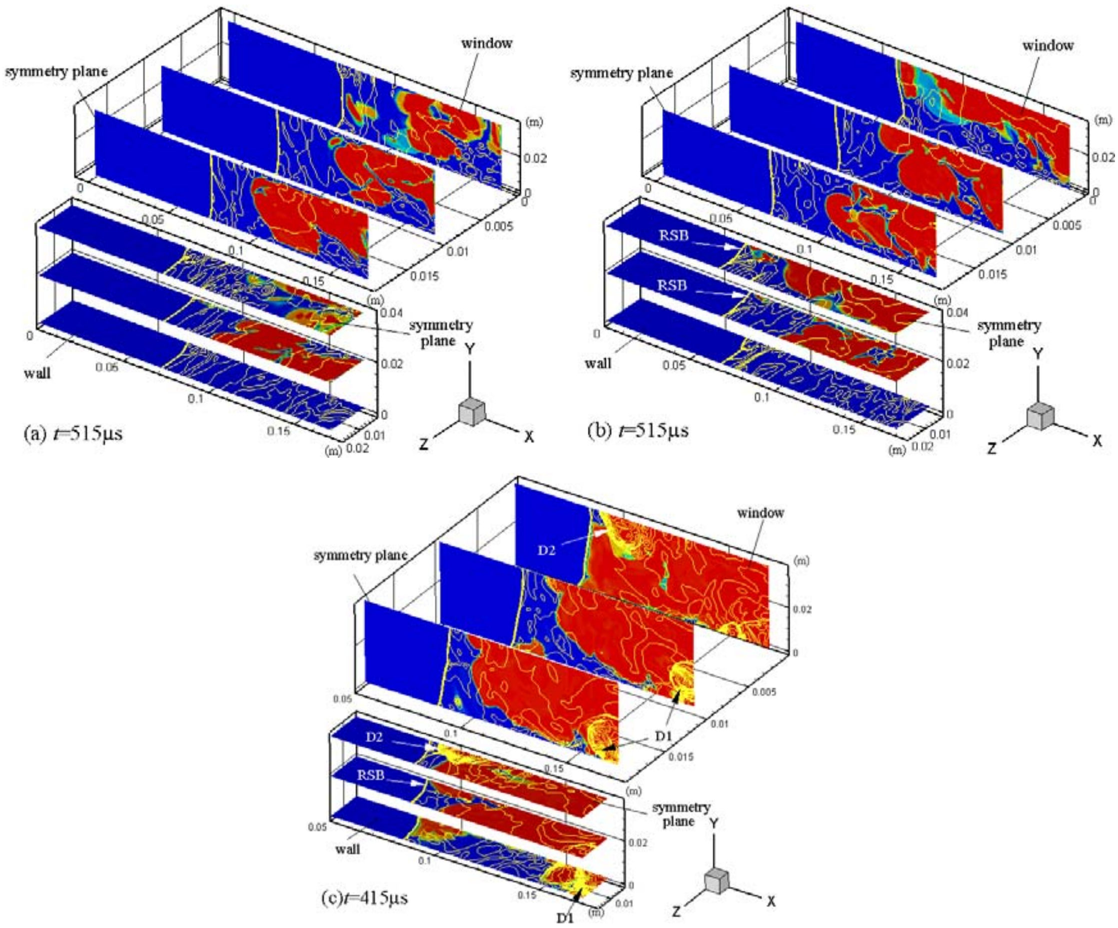


Figure 2. Fuel mass fraction distributions and pressure contours of distorted flames in shock accelerated flows at the selected times. (a) case 1, (b) case 2, (c) case 3. Red color corresponds to the unburned mixture, blue color corresponds to the burned mixture, yellow lines represent pressure contours. Reflected wave travels from right to left along $x$ direction.

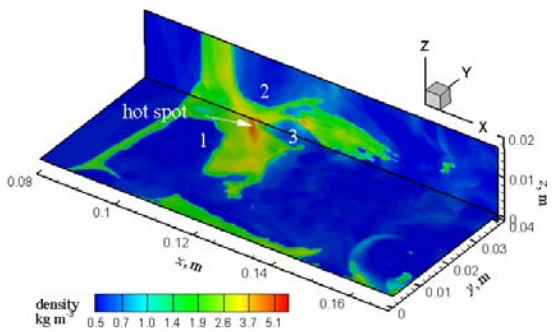


Figure 3. Density distributions in $z$=0.002m slice of $x$-$y$ plane and $y$=0.038m slice of $x$-$z$ plane show the formation of a hot spot for case 3, $t$=406μs.

To study the flame development and acceleration, Fig. 4 gives the flame volume normalized by initial volume, $V_0$, and flame mass burning rate, $\dot{m}$ , as functions of time for three cases. Fig. 4(a) shows that the initial spherical flames are firstly compressed by incident shock wave and then they slowly expand owing to combustion until the reflected wave hits the flame again. Once the reflected wave passes through the flames, they are compressed again and then rapidly expand. The typical process is also seen in Fig.1 for case 1. In Fig. 4(b), the burning rate of flames is greatly increased in the reflected wave flow compared with that in the incident shock flow. In particular, after the reflected wave passes through, the burning rate of flames for cases 1 and 2 are almost same, which implies that the spherical flame number has no significant influence on flame acceleration, while the burning rate of flame for case 3 increases dramatically, which suggests that the shock wave strength plays an important role in flame acceleration and detonation initiation.

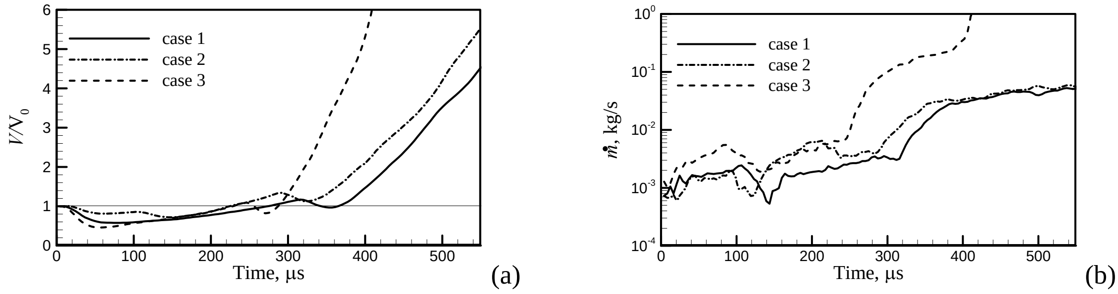


Figure 4. Time histories of (a) normalized volume and (b) mass burning rate for distorted flames at the different incident shock wave strengths and spherical flame numbers.

To further understand the effect of shock strength on the flame acceleration, Figs. 5(a) and 5(b) show the global heat release rate and vorticity of flames as functions of time. In Fig. 5(a), it can be seen that heat release rate of flames initially increases during the passage of incident shock wave and then becomes flat in the incident shock flow. After that, it rapidly increases during the passage of the reflected wave and then slowly increases in the reflected shock flow. These results mean that shock wave can greatly promote the heat release of flames due to the shock heat effect. Case 3 in the Fig. 5(a) has much higher heat release rate during the whole shock-flame interaction which suggests that the higher Mach number of incident shock wave greatly increases the temperature behind the wave and thus leads to faster reaction rate and much more chemical heat release. On the other hand, Fig. 5(b) gives the mean magnitude of vorticity within flames, $\overline{\omega} = \iiint \sqrt{\omega_x^2 + \omega_y^2 + \omega_z^2}\, dxdydz / V$ , as a function of time to represent the mixing strength of unburned/burned mixture by vortices induced by incident shock wave and its reflected wave, here $\omega_x$, $\omega_y$ and $\omega_z$ denote vorticity components in $x$, $y$ and $z$ directions, respectively, $V$ denotes the volume of flames. It can be found that two vorticity peaks are generated for each case when the incident shock and its reflected wave interact with flames respectively. The vorticity generation by baroclinic effect can enhance the mixing between the unburned gas and burned gas and then increase chemical reaction rate and heat release rate. The stronger shock wave results in higher vorticity which further enhances the mixing effect. Note that the vorticities become decrease after incident shock or its reflected waves has passed through the flames because the flame expansion and burn-out effect weaken the vorticity within the flame.

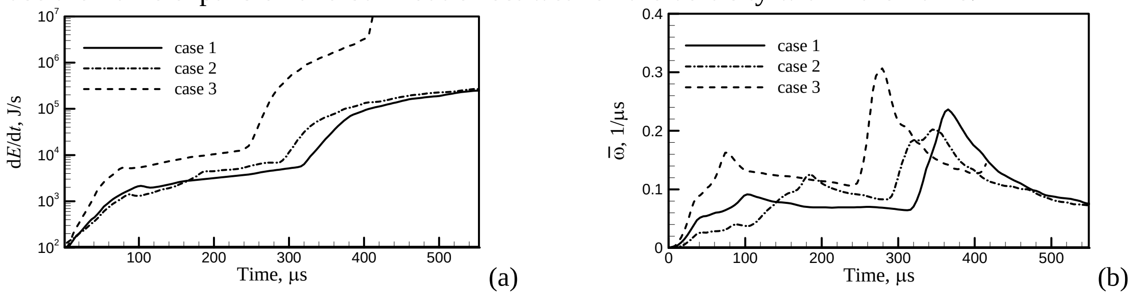


Figure 5. Time histories of (a) total heat release rate and (b) mean vorticity magnitude for distorted flames at the different incident shock wave strengths and spherical flame numbers.

# 4 Conclusions

In present study, the 3D spherical flames instability and acceleration induced by incident shock and its reflected waves are numerically studied for an ethylene-oxygen-nitrogen mixture. In particular, the effects of shock wave strength and spherical flame number on the shock-flame interaction are focused and investigated. The results show that the severe distortion and rapid acceleration of flames occur when the reflected shock wave has passed through the flames. The spherical flame number has no significant influence on the flame evolution. Compared with the single spherical flame case, a reactive shock bifurcation structure in the double spherical flames case more likely appears on the wall due to the larger total flame surface area. The shock wave strength has important influence on the flame instability and acceleration. The shock wave with higher strength can produce stronger reactive shock bifurcation which is related to formation of hot spot that leads to a detonation, while the shock wave with lower strength cannot lead to a detonation but only disturb and accelerate flame. Shock heating and vorticity generation during shock-flame interaction play the important roles in flame instability and acceleration, especially for incident shock and its reflected waves with high strength.

**Acknowledgements:** This work was supported by Natural Science Fund of China (No. 10972107).

## References

[1] Markstein GH. (1964). Non-Steady Flame Propagation. Macmillan, New York.

[2] Thomas GO, Bambrey R, BrownC. (2001). Experimental observations of flame acceleration and transition to detonation following shock-flame interaction. Combust. Theory Model. 5 : 573.

[3] Yang J, Kubota T, Zukoski EE. (1994). Applications of shock-induced mixing to supersonic combustion. AIAA J. 31: 854.

[4] Batley GA, McIntosh AC, Brindley J, et al. (1994). A numerical study of the vorticity field generated by the baroclinic effect due to the propagation of a planar pressure wave through a cylindrical premixed laminar flame. J. Fluid Mech. 279:217.

[5] Ju Y, Shimano A, Inoue O. (1998). Vorticity generation and Flame distortion induced by shock flame interaction. Proc. Combust. Inst. 27: 735.

[6] Gamezo VN, Oran ES, Khokhlov AM. (2005). Three-dimensional reactive shock bifurcations. Proc. Combust. Inst. 30: 1841.

[7] Oran ES, Gamezo VN. (2007). Origins of the deflagration-to-detonation transition in gas-phase combustion. Combust. Flame. 148: 4.

[8] Dong G, Fan BC, Ye JF. (2008). Numerical investigation of ethylene flame bubble instability induced by shock waves. Shock Waves. 17: 409.

[9] Dong G, Fan BC, Gui M, et al. (2009). Numerical simulations of interactions between a flame bubble with an incident shock wave and its focusing wave. J. Mech. Eng. Sci. 223:2357.

[10] Chakravarthy SR, Osher S. (1985). A new class of high accuracy TVD schemes for hyperbolic conservation laws. AIAA 23rd Aerospace Science Meeting. 85-0363.

[11] Khokhlov AM, Austin JM, Pintgen F, et al. (2004). Numerical study of the detonation wave structure in ethylene-oxygen mixtures. 42nd AIAA Aerospace Science Meeting and Exhibit. 2004-792.

[12] Austin JM. (2003). The role of instability in gaseous detonation. Dissertation (Ph.D.), California Institute of Technology, Pasadena, California.

[13] Kessler DA, Gamezo VN, Oran ES. (2010). Simulations of flame acceleration and deflagration-to detonation transitions in methane-air systems. Combust. Flame. 157: 2063.